Stretch-Triggered Drug Delivery from Wearable Elastomer Films Containing Therapeutic Depots

Jin Di,[†,‡,#] Shanshan Yao,[§,#] Yanqi Ye,[†,‡] Zheng Cui,[§] Jicheng Yu,[†,‡] Tushar K. Ghosh,[∥] Yong Zhu,[*,†,§] and Zhen Gu[*,†,‡,⊥]

[†]Joint Department of Biomedical Engineering, University of North Carolina at Chapel Hill and North Carolina State University, Raleigh, North Carolina 27695, United States, [‡]Center for Nanotechnology in Drug Delivery and Division of Molecular Pharmaceutics, UNC Eshelman School of Pharmacy, University of North Carolina at Chapel Hill, Chapel Hill, North Carolina 27599, United States, [§]Department of Mechanical and Aerospace Engineering, North Carolina State University, Raleigh, North Carolina 27695, United States, [∥]Fiber and Polymer Science Program, Textile Engineering, Chemistry, and Science Department, North Carolina State University, Raleigh, North Carolina 27695, United States, and [⊥]Department of Medicine, University of North Carolina at Chapel Hill, Chapel Hill, North Carolina 27599, United States. [#]J.D. and S.Y. contributed equally.

ABSTRACT Mechanical force-based stimulus provides a simple and easily accessible manner for spatiotemporally controlled drug delivery. Here we describe a wearable, tensile strain-triggered drug delivery device consisting of a stretchable elastomer and microgel depots containing drug loaded nanoparticles. By applying a tensile strain to the elastomer film, the release of drug from the microdepot is promoted due to the enlarged surface area for diffusion and Poisson's ratio-induced compression on the microdepot. Correspondingly, both sustained drug release by daily body motions and pulsatile release by intentional administration can be conveniently achieved. Our work demonstrated that the tensile strain, applied to the stretchable device, facilitated release of therapeutics from microdepots for anticancer and antibacterial treatments. Moreover, polymeric microneedles were further integrated with the stretch-responsive device for transcutaneous delivery of insulin and regulation of blood glucose levels of chemically induced type 1 diabetic mice.

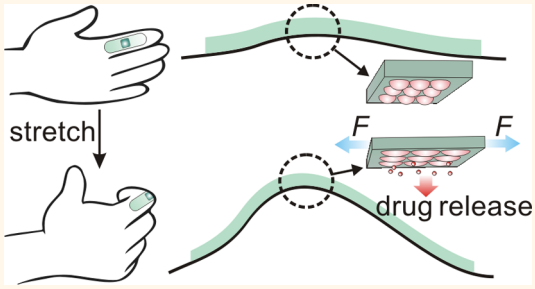

KEYWORDS: drug delivery · wearable devices · stimuli-responsive · nanoparticles · microdepots

The stimuli-triggered drug delivery system, which enables a dose-, spatial- and/or temporal-controlled release fashion, plays an indispensable complementary role to the sustained release systems.[1,2] To date, numerous "smart" formulations have been developed based on a variety of stimuli, which can be physiological signals, such as pH,[3] redox potential,[4] ATP gradient,[5] enzymatic activities[6,7] and glucose levels,[8,9] or external physical triggers, such as light,[10] temperature,[11] ultrasound,[12] magnetic field[13,14] and electric current.[15] However, the clinic translation of the methods based on the physiological changes-associated stimuli is often challenged by the difficulty of a precise dose control in the complicated physiological environment,[16] while the external trigger-mediated methods are limited by a need of additional instrumentation.

Mechanical strain-based stimulus, accompanying with ubiquitous daily motions, could offer a simple and easily accessible manner for promoting drug release spatiotemporally. Such strain variations can be readily achieved by tension in muscles, organs, tendons and bone joints, compression in cartilage and bones, or shear force in blood vessels.[17] In addition, strain-triggered delivery system holds promise for self-administration of releasing analgesic or emergency drugs through simple body motions. Despite these, very few strain-triggered drug delivery methods have been developed, mainly utilizing compression. For example, Mooney and co-workers[17,18] demonstrated compression-controlled release of a vascular endothelial growth factor from alginate hydrogels. Increased pressure within the polymer matrix dissociated/depleted the drugs and enabled an enhanced release under a compression force. In another work, mild mechanical compressions were employed to reduce the inclusion

* Address correspondence to zgu@email.unc.edu, yong_zhu@ncsu.edu.

Received for review June 29, 2015 and accepted August 5, 2015.

Published online August 10, 2015
10.1021/acsnano.5b03975

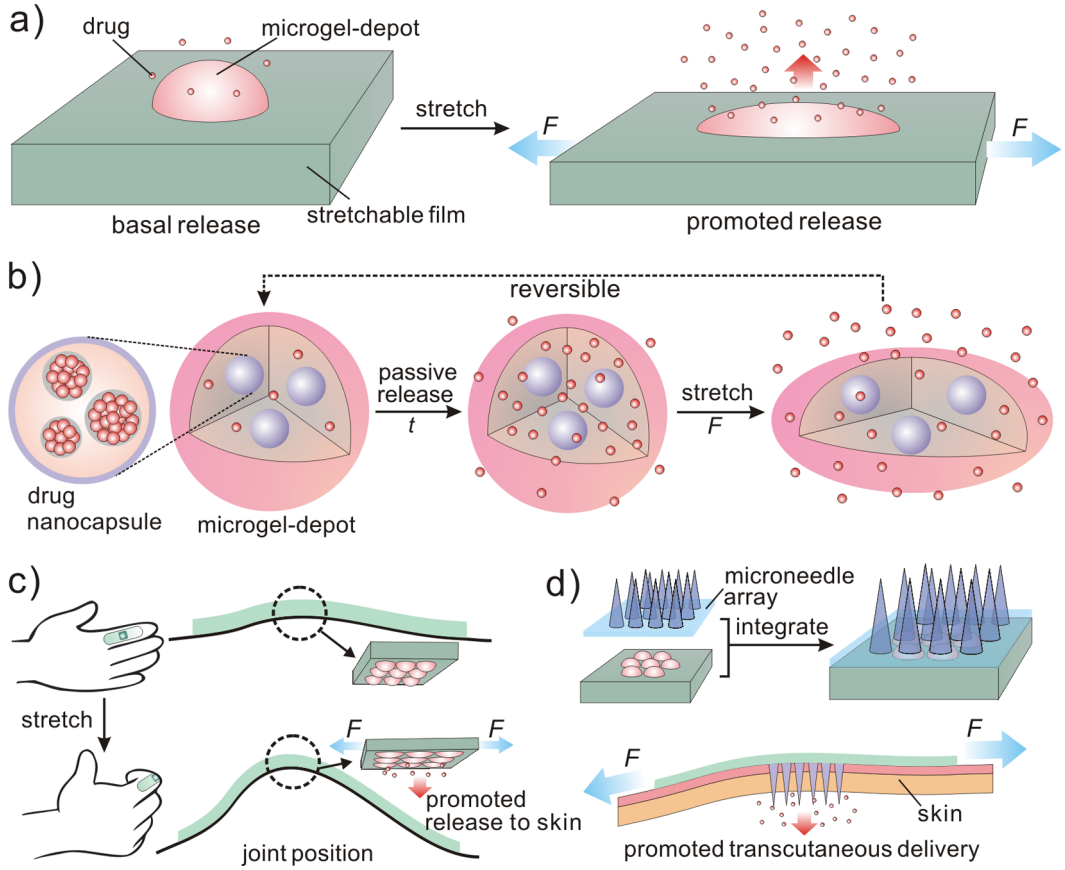

Figure 1. Schematic illustration of the tensile strain-triggered drug release. (a) The microdepot follows the deformation of the stretchable elastomeric substrate under stretching, which facilitates the drug release from the microdepot. (b) Drug slowly diffuses from the NPs into the microdepots. The tensile strain promotes the drug release from the microdepots. (c) Drug loaded wearable devices can be attached conformally to the finger with the microdepots area on the finger joint. Finger flexion triggers the promoted release to the skin. (d) The drug loaded wearable device integrates with a microneedle array patch. Stretching of the device promotes the drug release from microdepots, which further diffuses into the needle for transcutaneous delivery.

ability of the host molecule networks and thus accelerated the release of the antiemetic drug (guest molecule) from hydrogels (host molecule).[19] Jeong and co-workers[20] fabricated a drug-containing buckling polymer thin film on an elastomeric substrate. Upon stretching with a maximum strain of 7.5%, the volume of the buckled "container" decreased, resulting in release of the preloaded molecules. However, the low strain tolerance restricts their use in applications involving large deformations. For example in wearable applications, the strain can reach as large as 50%. A stretchable delivery system with large deformation and high drug loading capacity for long-term treatment remains elusive.

Herein we report a wearable,[21−24] tensile strain-triggered drug delivery device. As shown in Figure 1a−c, the cross-linked microgels containing drug-loaded polymeric nanoparticles (NPs) serve as depots for sustained drug release, while a highly stretchable elastomer (Dragon Skin 30) integrated with "microdepots" serves as a substrate for loading tensile strain. The encapsulated drug in NPs is passively released and partially detained in the matrix of the microdepots. Once a tensile strain is applied, the release of drug from the microdepot is promoted due to the enlarged surface area for diffusion and Poisson's ratio-induced compression on the microdepots. Our work demonstrated that the tensile strain, applied either by daily joint motions or intentional stretching, was effective to promote the release of therapeutics for antibacterial and anticancer treatments. Microneedles were further integrated with the stretch-responsive device for transcutaneous delivery of insulin to regulate blood glucose levels of type 1 diabetic mice.

RESULTS AND DISCUSSION

Device Fabrication and Characterization. To test our concept of the stretch-triggered drug delivery device, doxorubicin hydrochloride (DOX), a chemotherapeutic drug used to treat a wide spectrum of cancers, was applied as a model drug. To encapsulate DOX, the poly(lactic-*co*-glycolic acid) (PLGA) NPs were prepared *via* a double-emulsion (w/o/w)-based solvent evaporation/extraction method.[25] The resulting NPs have diameters of 256.9 ± 19.9 nm and zeta potentials of −53.8 ± 3.2 mV (Figure 2a). Next, the NPs were encapsulated in the alginate microgels *via* the

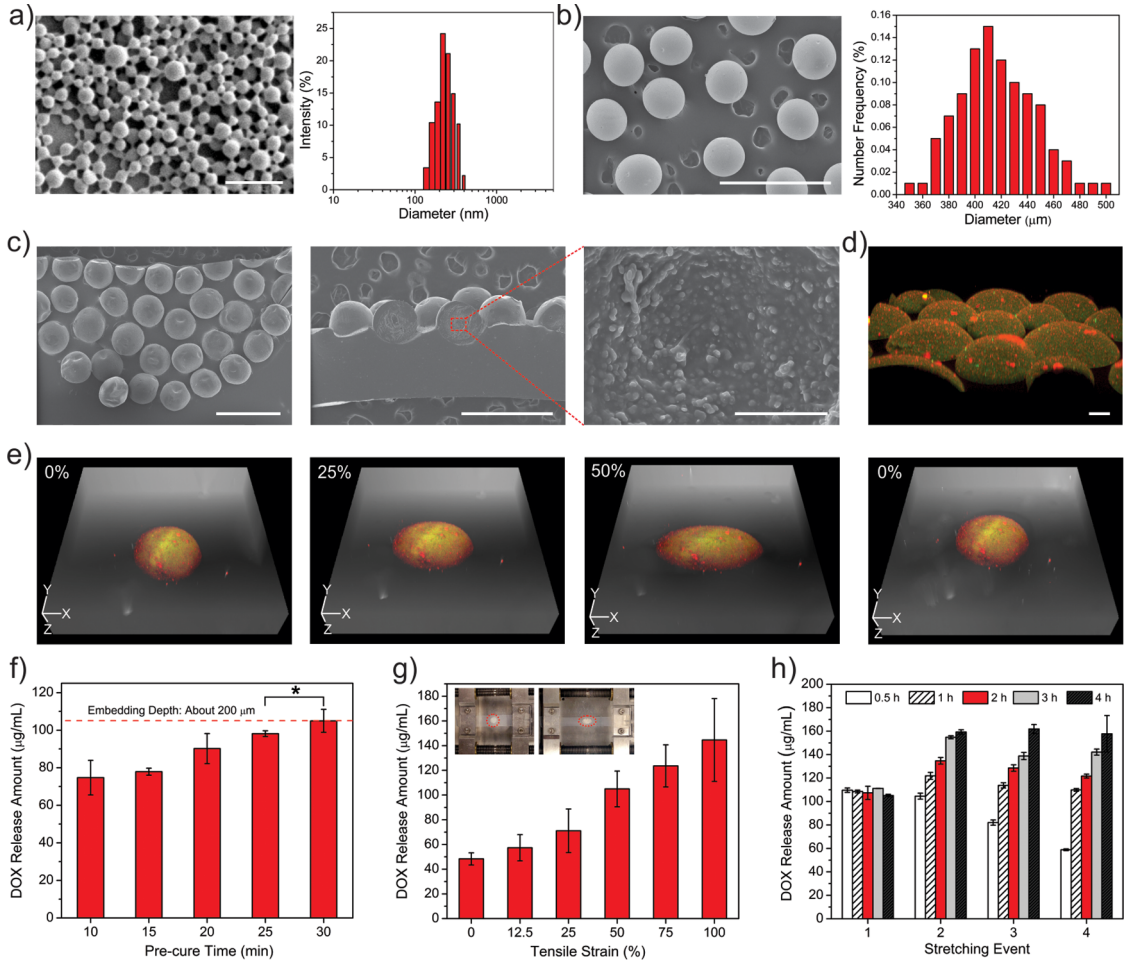

Figure 2. Characterizations of the DOX-loaded PLGA NPs, microdepots encapsulated with PLGA NPs and stretchable elastomers embedded with microdepots. (a) SEM image of the PLGA NPs (scale bar: 1 μm) (left) and the size distribution of the NPs (right). (b) SEM image (left) and size distribution (right) of NP-encapsulated microdepots. Scale bar: 1 mm. (c) Top-view (left) and cross-sectional (middle) SEM images of a stretchable elastomer embedded with microdepots. Scale bars: 1 mm. The right shows a high magnification SEM image of the interior of a NP-encapsulated microdepot. Scale bar: 50 μm. (d) Laser scanning confocal microscopy (LSCM) image of the FITC-tagged microdepots encapsulated with DOX loaded PLGA NPs. Scale bar: 100 μm. (e) LSCM images of a microdepot embedded in elastomeric substrate when the substrate was in the initial state (zero strain), under 25% strain, under 50% strain and went back to zero strain, respectively. Scale bars: 100 μm (*X*, *Y*, *Z* direction). (f) The released amount of DOX from the devices as a function of precuring time of the liquid elastomer before embedding the microdepots. Ten cycles of tensile strains at 50% with the speed of 2 s/cycle were applied. (g) The released amount of DOX from the devices under different tensile strain levels, ranging from 0 to 100%. Precure time was 30 min and 10 cycles of stretching and releasing were applied for each strain level with the speed of 2 s/cycle. The insets show the device mounted on the tensile stage before (left) and after (right) applying strain. The red dash circles indicate the positions with microdepots. (h) *In vitro* release of DOX from DOX-formulated devices with different intervals (0.5−4 h) between each stretching event. For each event, 10 cycles of stretching at 50% strain were applied. Data presents mean ± SD (n = 3). *P < 0.05 (*t*-test).

electrospray method, cross-linked by barium chloride ($BaCl_2$).[26] The size of the obtained microdepots is 406.2 ± 14.5 μm in diameter (Figure 2b). Commercially available high performance silicone Dragon Skin 30 was selected as the elastomeric substrate due to its high stretchability (360%) and the ability to cure at room temperature for maintaining the bioactivity of encapsulated drugs. More information on Dragon Skin 30 is available in the datasheets.[27] The microdepots can be embedded halfway into the stretchable Dragon Skin elastomer substrate (Figure 2c). Successful encapsulation of DOX in microdepots was verified by the laser scanning confocal microscopy (LSCM). As shown in Figure 2d, DOX-loaded PLGA NPs were encapsulated by FITC tagged alginate microdepots with homogeneous distribution. To visualize the deformation change of the microdepots in response to tensile strain, the 3-dimentional (3-D) confocal images of the microdepots at different strain levels, from zero to 50% and then back to zero strain, were acquired (Figure 2e). Upon longitudinal stretching of the elastomeric substrate, the embedded microdepots followed the geometric change of the Dragon Skin substrate: they elongated in the length direction and shrank in the width and height directions. After releasing the applied strain, the microdepots recovered most in shape with a slight residue deformation, which corresponded to about 10% of the tensile strain in the length direction.

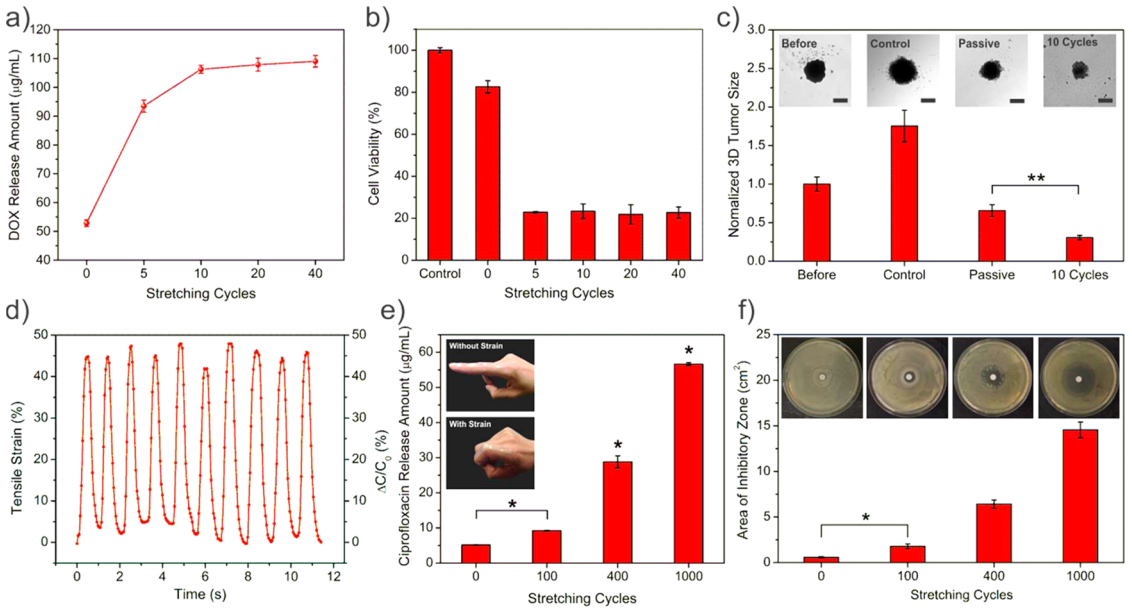

Figure 3. ***In vitro*** **anticancer effects and bactericidal applications of the wearable device. (a)** ***In vitro*** **release of DOX from DOX-formulated devices after 0, 5, 10, 20, and 40 cycles of stretching at 50% strain. (b) Cell viability of HeLa cells 24 h post-treatment by media collected from DOX-formulated device after 0, 5, 10, 20, and 40 cycles of stretching at 50% strain. Cells without treatment were used as a negative control. (c) Normalized HeLa tumor spheroid sizes and morphologies (insets) before treatment (before), without treatment (control), treated with media collected from DOX-formulated devices after 10 cycles of stretching (10 cycles), and treated with media collected from DOX-formulated devices without stretching (passive) after 3 days. Scale bars: 100 μm. (d) Strain and relative capacitive changes associated with finger flexion measured by the capacitive sensor shown in Figure S4 inset. (e) Antibacterial assay using released ciprofloxacin solutions during 100, 400, and 1000 cycles of finger flexions. Passive released ciprofloxacin (without placing on finger and without strain) was included for comparison. The insets show the pictures of a wearable device on finger with the microdepot embedded area on the finger joint. Finger flexion offered the tensile strain to facilitate the release of ciprofloxacin. (f) The images and the diameters of the inhibitory zone produced around the paper disk measured after incubating for 24 h at 37 °C. 50 μL of sample solutions were applied to the sterilized filter paper disks with diameter of 5 mm. The ciprofloxacin diffused from the disk to inhibit *E. coli* growth. Data represents mean ± SD (n = 3). *P < 0.05 (t-test), **P < 0.01 (two-tailed t-test).**

The elastomer (Dragon Skin) started in the liquid phase with a low viscosity; its viscosity increased with time during precuring at room temperature. The microdepot embedding depth can be adjusted by controlling the precuring time (*e.g.*, 10 to 30 min in our experiments). After loading the microdepots, the elastomer was further cured for 16 h to solidify the liquid. To quantify the released drug, the devices were mounted onto a mechanical stage (Figure 2g inset) to apply 10 cycles of 50% tensile strain with a speed of 2 s/cycle. 50 μL phosphate buffered saline (PBS) solution was dropped onto the microdepots area to collect the released drug. A shallower embedding depth under a longer precuring time led to a larger volume of the microdepots that was surrounded by the PBS solution. As shown in Figure 2f, the amount of the released DOX increased with the precuring time for up to 30 min, which corresponded to the case that the spherical microdepots being embedded about halfway inside the elastomeric substrate (Figure 2c). The embedding depths for precuring time higher than 30 min were too shallow to securely bond the microdepots within the elastomeric substrate. As a result, the microdepots could detach from the substrate under stretching. The amount of released drug was also dependent on the strain levels applied to the elastomeric substrate. Tensile strain can effectively stimulate the release, with an increase in the release amount at a higher strain (Figure 2g). Although strain level at or higher than 75% resulted in a higher release rate, such a high strain caused the irreversible cracking of the microdepots, as shown in Supporting Information, Figure S2. Furthermore, most of the human motions, such as bending of the knees, finger joints and wrists, typically do not involve strain higher than 50%.[28,29] Taken together, a precure time of 30 min for the device fabrication and a tensile strain of 50% were chosen for following studies.

In addition to the microdepot embedding depth and the strain level that was applied onto the microdepots, the third critical parameter controlling the drug release is the time interval between each stretching event. Here, 10 continuous stretching cycles are designated as one stretching event. To identify the smallest effective interval for a pulsatile release profile, after the initial 10 stretching cycles (Figure 3a), the subsequent stretching events were performed with various intervals, ranging from 0.5 to 4 h. The release of DOX for four events with different intervals is presented in Figure 2h. Due to the relatively slow diffusion rate of drug from

NPs to microdepots, insufficient interval leads to rapid depletion of a corresponding small amount of drug stored in the microdepots before the following stretching events. The results showed that an interval of 4 h was sufficient for the drug to "recharge" in the microdepots.

Test of Stretch-Mediated Drug Release and Analysis of Mechanism. Figure 3a shows the release profile of DOX during consecutive stretching and releasing cycles. Ten cycles of stretching led to 2-fold higher release amount compared to the passive release from the unstretched device. After 10 cycles, an insignificant increase in release rate was observed when more stretching cycles were applied. The *in vitro* therapeutic effectiveness of the strain-stimulated drug release device was evaluated next. As displayed in the antiproliferation profile of HeLa cells (Figure 3b), the sample solution collected from stretched devices exhibited much higher cytotoxicity compared with that from unstrained ones. Moreover, the media from devices experienced 10 cycles of 50% tensile stretching were used for a tumor spheroid growth inhibition study (Figure 3c). The tumor spheroids treated with the sample solution collected from the stretched devices exhibited a more significant reduction in size with loose intercellular junctions after 3 days, compared to the control groups without treatment or treated with the sample solution from the unstretched devices.

On the basis of the results of DOX described above, it can be seen that tensile strain stretches the microdepots in the axial direction and promotes the drug release from the microdepots. Here we further investigate the mechanism of the stretch-mediated drug release. A microdepot, initially a sphere, deforms to an ellipsoid under tensile strain. Once a droplet of aqueous solution is in contact with the top half of the microdepot that contains high-concentration drugs diffused from the encapsulated NPs, the concentration gradient drives the drugs to diffuse from the microdepot to the aqueous solution. In reality, the diffusion from the microdepot surface is between two extreme cases—constant-source diffusion and limited-source diffusion—depending on the replenishment rate from the inner layers. Assuming the volume of the microdepot and the total drug dose in the microdepot do not change with the stretching, the initial drug concentration in the microdepot before and after the stretching should remain constant. For either of the two diffusion modes, the diffusion rate is proportional to the surface area.[30,31] Since a sphere has the smallest surface area for the same volume, the diffusion rate increases after the stretching. In addition, the elastomeric substrate has a larger Poisson's ratio than the porous microdepot,[32,33] hence the substrate tends to shrink more in the transverse directions, leading to a compressive force on the embedded part of the microdepot (Supporting Information, Figure S3). In short, the enhanced drug delivery under stretching can be attributed to the enlarged surface area of the microdepot in contact with the aqueous solution and the Poisson's ratio induced compression on the microdepot.

Bactericidal Efficacy of the Wearable Device. Next, to test the potential of utilizing body motions for promoting drug release in a stretch-mediated manner, ciprofloxacin (CIF), a potent broad-spectrum antibiotic to treat infections, was incorporated into the device for sustained treatment of the local infection. The device formulated with CIF was simply attached to the finger and made a conformal contact with the microdepots on the finger joint. When the finger flexed, the device attached at the finger joint was stretched for multiple cycles to stimulate the drug release. To quantify the tensile strain associated with finger motions, a silver nanowire (AgNW) based capacitive strain sensor was integrated with the CIF-formulated device (Supporting Information, Figure S4 inset) to record the strain associated with finger flexion in real time. The capacitive sensor consists of two conductors made from AgNWs embedded just under the surface of Dragon Skin elastomer and a thin layer of Ecoflex 00−10 as the dielectric sandwiched in between. When the finger flexes, the area of the capacitive strain sensor increases while the separation between two electrodes decreases, resulting in an increases in capacitance.[28] The capacitive was calibrated to have a gage factor of 1, as shown in Supporting Information, Figure S4. The maximum strain involved with the finger flexion measured by the sensor was found to be around 45% (Figure 3d). To facilitate the comparison among the drug release for various stretching cycles, the finger was fully flexed to have a comparable flexion angle and strain for each cycle. To assess the release efficacy, the solutions containing released drug were collected from passive release (no stretching event), 100, 400, and 1000 cycles of finger flexions and their antibacterial performances were compared toward *E. coli* using the disk diffusion method. In Figure 3e and 3f, the sample solution of passive release had the lowest amount of released drug (5.2 μg/mL) and correspondingly, a smallest inhibitory zone of 0.05 cm^2 was achieved. In contrast, the amount of drug released upon finger movements for 100, 400, and 1000 times significantly increased (9.2, 28.8, and 56.6 μg/mL, respectively) and larger killing areas of bacteria (1.78, 6.41, and 14.56 cm^2 respectively) were observed. This clearly indicated that increasing cycles of finger movements were able to facilitate the drug release steadily, leading to an enhanced antibacterial efficacy. This demonstration validated the potential of utilizing the stretchable device for substantial release of therapeutics, such as anti-inflammatory, anti-infective agents and pain reliever, simply triggered by daily human motions.

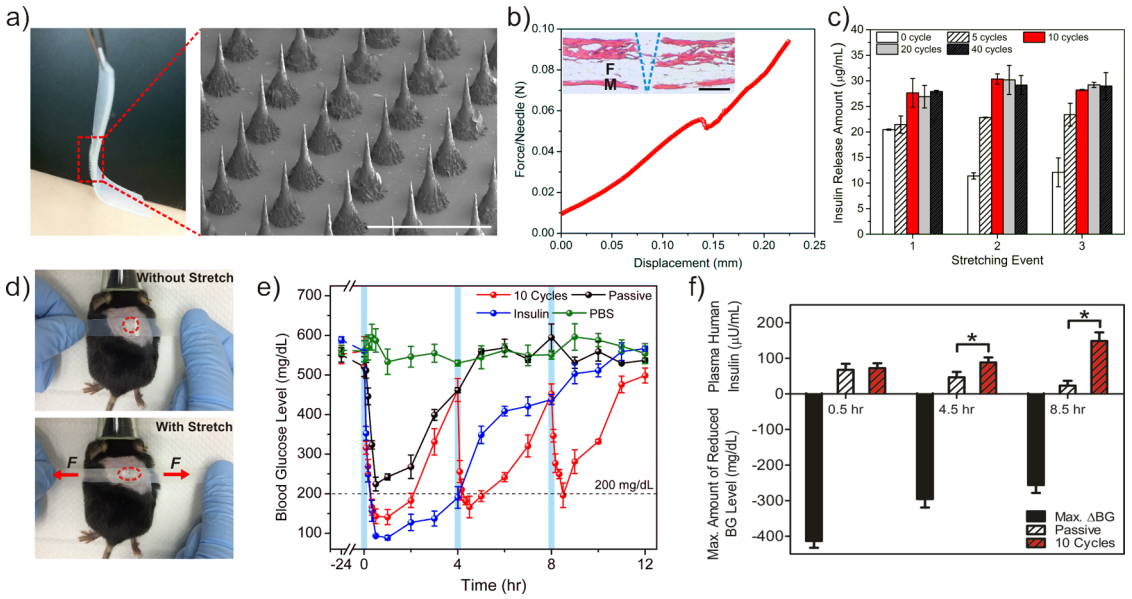

Figure 4. ***In vitro*** **and** ***in vivo*** **studies of the stretch-mediated blood glucose (BG) level regulation for STZ-induced diabetic mice using microneedle integrated device. (a) A picture of the microneedle integrated wearable device (left) and SEM image of a microneedle array (right). Scale bar: 1 mm. (b) Compressive force applied on each needle as a function of displacement by pressing the microneedle array against a stainless steel plate. The inset shows the section of the hematoxylin and eosin (H&E) stained mouse skin that was penetrated by a microneedle. Blue dashed line indicates the original microneedle insertion site. "M" and "F" indicate the regions of skin muscles and fat tissues, respectively. Scale bar: 100 μm. (c)** ***In vitro*** **release of insulin from the microneedle integrated device after 0, 5, 10, 20, and 40 stretching cycles at 50% strain with an interval of 4 h. (d) Photos of a microneedle integrated insulin-formulated device applied on shaved dorsal skin of a mouse without (top) and with (bottom) strain. The tensile strain was provided by stretching the device using two hands. The red dash circles indicate the positions of microdepots with microneedles. (e) The BG levels of STZ-induced diabetic mice after (1) wearing devices with 10 cycles of 50% stretching with an interval of 4 h by hand (red line), (2) wearing devices without stretching (passive) (black line), (3) being subcutaneously injected with insulin solution with a same dose as applied into the microdepots used in (1) and (2) (blue line), and (4) being subcutaneously injected with PBS solution only (green line) (n = 4). The BG levels were continuously monitored in predetermined time with a 4 h interval. (f) Changes of the plasma insulin concentration and maximum of reduced BG levels over time after initial application and after each stretching event. Data represents mean ± SD. *P < 0.05 (t-test).**

Insulin Delivery Using the Wearable Device. To further broaden the utility of the wearable drug delivery devices for transcutaneous drug delivery, insulin was formulated into the device. For the traditional administration methods for type 1 and advanced type 2 diabetes,[34] patients need to perform subcutaneous injection of insulin several times a day, which is painful and can cause infection, tenderness, nerve damage and ultimately local tissue necrosis. Here, we integrated the insulin-containing microdepots embedded wearable device with painless microneedles, made by cross-linked hyaluronic acid (HA) (Figure 4a). The fracture force of the cross-linked microneedles was determined as 0.06 N/needle, suggesting sufficient strength for skin penetration without breaking the needle. Hematoxylin and eosin (H&E) stained section of a mouse skin confirmed the successful penetration of microneedle (Figure 4b).[35] The triggered released insulin was expected to diffuse into the transcutaneous microneedles and be delivered into the regional lymph and capillary vessels.[36] As shown in Figure 4c, the amount of insulin released *in vitro* from the stretchable device saturated after 10 cycles (2 s/cycle) of stretching at 50% strain. Moreover, with an interval of 4 h, approximately the same amount of released insulin was recorded in several continuous stretching events. The circular dichroism (CD) spectrum[9] showed that the secondary conformational structure of released insulin from microdepots and microneedles integrated wearable devices did not change compared to that of the native insulin[37] (Supporting Information, Figure S5). To evaluate the *in vivo* performance of the insulin-loaded device for treating diabetes, streptozotocin (STZ)-induced type 1 diabetic mice were divided into four groups and subjected to different treatments: (1) wearing devices with 10 cycles of 50% stretching by hand (Figure 4d), (2) wearing devices without stretching, (3) subcutaneous injection with insulin solution with a same dose as applied into the microdepots used in (1) and (2), and (4) subcutaneous injection with PBS solution only. The blood glucose (BG) levels of mice were monitored over time using a glucose meter at predetermined time points. As shown in Figure 4e, after each stretching event (10 cycles of stretching with strain level of 50%) with an interval of 4 h, the BG levels of mice declined rapidly to a normoglycemic state (<200 mg/dL) within 30 min and then gradually increased. The pulsatile and continuous reduction of BG levels was observed upon the three stretching events. Whereas in the absence of stretching, the BG

levels decreased due to the initial burst release of insulin at the beginning, but with insufficient insulin amount, the BG levels maintained in the hyperglycemic range. Similarly, the direct injection of insulin with a relatively high dose caused rapid reduction of BG levels, which had a risk of hypoglycemia, and the BG levels recovered to the hyperglycemic state after 4 h. Correspondingly, for the mice wearing the device and subjected to stretching, the plasma insulin concentration in the mice maintained at a relatively high level after each stretching event, while that of the mice in the unstrained group rapidly decreased after the initial administration, as quantified by the enzyme-linked immunosorbent assay (ELISA) (Figure 4f). Additionally, H&E stained skin sections with surrounding tissues were examined. There was no obvious inflammation observed in the region on day 2 postadministration (Supporting Information, Figure S6).[37] Of note, long-acting insulin or glucagon-like peptide-1[38] can be further incorporated to tune the pharmacokinetics and regulate the BG levels correspondingly.

CONCLUSIONS

In summary, we developed a wearable tensile strain-triggered device consisting of a stretchable elastomer and microdepots containing therapeutics, the drug release of which can be promoted by body motions. Either sustained release by daily motions of muscles, tendons and bone joints or pulsatile release by intentional administration (such as using hands) can be achieved in a convenient manner. This skin-mountable device has the potential of substantially releasing anti-inflammatory, anti-infective agents or painkiller to the skin. Combining with microneedle arrays, this device can be utilized to deliver small drug, hormone or vaccine to the body through transcutaneous administration. In addition, a potential organ motion-triggered device for enhanced anticancer therapy or tissue regeneration is also expected based on this device. Furthermore, this device can also be integrated with other wearable modality to sense the real-time physiological signals, such as electrocardiograph, blood glucose levels or body temperature and provide feedback to guide the precise drug delivery.[39−41]

METHODS

Materials. PLGA (lactide:glycolide (50:50), MW: 40−75 kDa), anhydrous dichloromethane (DCM), sodium alginate, barium chloride dihydrate, 1,6-diaminohexane, *N*-(3-(dimethylamino)-propyl)-*N*′-ethylcarbodiimide hydrochloride (EDC), *N*-hydroxysulfosuccinimide sodium salt (NHSS), fluorescein isothiocyanate (FITC, isomer I) and ciprofloxacin (CIF) were obtained from Sigma-Aldrich. Recombinant Human Insulin (Zn salt, 27.5 IU/mg) was purchased from Life Technologies. Doxorubicin hydrochloride (DOX) was obtained from Fisher Scientific. The deionized (DI) water was prepared by a Millipore NanoPure purification system (resistivity higher than 18.2 MΩ cm^{-1}). All chemicals were reagent grade and used as received.

Preparation and Characterization of the Alginate Coated PLGA Nanoparticles (NPs). DOX/CIF/insulin encapsulated NPs were prepared *via* a double-emulsion method.[25] Briefly, 4.5 mL organic phase DCM containing 180 mg PLGA was emulsified with 0.5 mL aqueous phase containing 5 mg Dox/15 mg CIF/30 mg insulin followed by sonication for 40 cycles (1 s each with a duty cycle of 40%). Then the primary emulsion was immediately poured into 25 mL 1 wt % alginate aqueous solution followed by the same sonication procedure. The double emulsion was subsequently transferred into 150 mL 0.2 wt % alginate aqueous solution. The mixed suspension was stirred at room temperature to eliminate DCM by evaporation. After 2 h, the resulting NPs were washed and collected by repeating the procedures of centrifuging at 10 000 rpm and suspending in DI water three times. The particle size was measured by dynamic light scattering (DLS). The zeta potential of the NPs was determined by their electrophoretic mobility using the same instrument after appropriate dilution in DI water. Measurements were made in triplicate at room temperature. NPs morphologies were investigated by a scanning electron microscopy (SEM) (JEOL 6400F, Tokyo, Japan) operated at 20 kV.

Synthesis of FITC-Alginate Derivative. Sodium alginate (120 mg) was mixed with 1-ethyl-3-(3-(dimethylamino)propyl)carbodiimide (EDC)/*N*-hydroxysuccinimide (NHS) (50 mg/30 mg) in pH 5.0 acetic buffer for 30 min to activate carbonyl groups on alginate, followed by mixing with additional 1,6-diaminohexane (60 mg) for another 4 h. The mixture was precipitated in 2-propanol (IPA) to remove unreacted diamine. The alginate-amine derivative was reacted with FITC (0.5 mg) in sodium bicarbonate solution (50 mM; pH = 8.5) for 4 h and precipitated in acetone to remove the unreacted FITC. The resulting FITC-alginate derivative was dissolved in DI water. Labeled alginate was mixed with 50 g of 2 wt % unlabeled sodium alginate solution and then the mixture was made into microspheres using the following process.

Fabrication and Characterization of Alginate Hydrogel Microdepots Loaded with NPs. An aqueous solution of 2 wt % alginate was centrifuged at 12 000 rpm to remove any impurities. Drug loaded PLGA NPs were added and thoroughly mixed with the alginate solution. The weight ratio of alginate/PLGA/DOX was 1/90/2.5, alginate/PLGA/CIF was 1/90/7.5 and alginate/PLGA/insulin was 1/90/15, respectively. The homogeneous mixture was vacuumed for 30 min before being transferred into a 5 mL syringe with an attached blunt tip, 22 gauge metal needle. The syringe was placed in an electrospray system equipped with a syringe pump. The positive electrode of the electrospray system was connected to the needle, and the negative electrode was connected to a metal receiving container with 50 mL of 20 mM $BaCl_2$. The solution was sprayed at a 0.155 mL/min flow rate under a high voltage (8 kV) with a working distance of 5 cm to the receiving container. The particles were cross-linked in $BaCl_2$ bath solution for 5 min before being collected. The collected microdepots were then rinsed three times with DI water by successive centrifugation cycles and stored at 4 °C after lyophilized. FITC alginate derivative was added into alginate solution to facilitate the laser scanning confocal microscopy (LSCM) (Zeiss LSCM 710, Carl Zeiss Micro Imaging, NY, USA). Microdepots sizes were determined by measuring the size of the particles under an optical microscope. The structural conformation of NPs loaded microdepots was observed using SEM. To prepare for SEM, microdepots were initially suspended in DI water. After they were dispersed, the microdepots were dehydrated in a series of ethanol solutions (20, 40, 60, 80, 90, 95, 100%) and then sputter-coated with gold/palladium. The LSCM was used to visualize FITC labeled alginate microdepots loaded with NPs (encapsulated with DOX). Sections of the confocal two-dimensional (2-D) slice images were generated from the top to the depth of 100 μm for each specimen. Afterward, ZEN software (Carl Zeiss MicroImaging, NY, USA) was used to reconstruct the three-dimensional (3-D) images.

Preparation of the Microdepot Integrated Wearable Device. The preparation of the wearable microdepot integrated device started with coating of a self-sticky silicone layer onto a microscope glass slide (Fisher Scientific, USA). Another layer of Dragon Skin 30 with part A to part B weight ratio of 1:1 was cast on top of the previous self-sticky layer and then cured at room temperature for 16 h. A strong bonding could be formed between the two layers. Biopsy punches (Miltex, USA) with a diameter of 5 mm were used to punch a circle in the middle of the elastomer (through two layers to the glass substrate). Following that, liquid Dragon Skin 30 precursor with the same ratio of part A to part B was used to fill in the punched area. After precuring the liquid at room temperature, drug-containing microdepots were loaded onto the liquid area. The liquid was fully cured after another curing time of 16 h with the drug-containing microdepots half-embedded within the elastomer. Since only the liquid dragon skin could securely embed the microdepots, the microdepots were confined to the punched circular area. Excess microdepots outside of the defined area were removed by tape. The final concentration of each bioactive agent within the device was as follows: DOX, 75 μg per device; CIF, 225 μg per device; insulin, 450 μg per device. The surfaces and cross sections of the microdepot incorporated devices were sputter-coated with gold/palladium and their morphologies were examined by the same SEM.

Fabrication of Methacrylate Modified Hyaluronic Acid (*m*-HA) Microneedle Integrated Device.[37] The microneedle fabrication was carried out using 5 uniform silicone molds from Blueacre Technology Ltd. Each mold is characterized with an 11 by 11 array of conical cavities machined by laser ablation. Enzymatically degradable hyaluronic acid (HA) was modified with methacrylated pendants according to our previous publication.[42] 50 μL (w/v = 40%) of methacrylated sodium hyaluronic acid, photo initiator (w/v = 1%) Irgacure-2959 and cross-linker *N*,*N*-Methylenebis(acrylamide) (MBA) (w/v = 40%) were mixed and deposited into the silicone cavities. The micromolds were placed under a vacuum (60 kPa) for 30 min to ensure that enough hydrogel could flow into the cavities. For better microneedles morphology, a piece of 4 cm $\times$ 9 cm silver adhesive tape was attached around the 2 cm $\times$ 2 cm micromold baseplate. 1.5 mL of mixed *m*-HA solution was added to the prepared micromold reservoir and the *m*-HA solution was dried at 25 °C for 6−8 h under vacuum desiccation. After desiccation was completed, the microneedle arrays were cross-linked through exposure to UV light for a short period of time and then carefully separated from the silicone mold. The mechanical strength of the microneedles were measured by compressing a stainless steel plate against microneedles using a stress−strain gauge. The speed of the top stainless steel plate toward the microneedle-array patch was 0.1 mm/s. The failure force of the microneedle was recorded when the needle began to buckle. To determine the skin penetration efficiency, the treated skin and the applied microneedle-arrays were imaged by a bright field microscopy. Briefly, the microneedle-array was applied to the dorsal skin of the mouse for 30 min. Mouse was then euthanized by CO_2 asphyxiation and the surrounding tissues were excised. The tissues were fixed in 10% formalin, then embedded in paraffin, cut into 5 μm sections, and stained using H&E for histological analysis. The images were obtained by an optical microscopy (Leica EZ4 D stereo microscope). The microneedle and wearable drug-loaded device were integrated together using silicone adhesive with microneedles sitting right on top of the microdepot region.

***In Vivo* Studies Using STZ-Induced Diabetic Mice.** The efficacy of the insulin-loaded devices for diabetes treatment was evaluated *in vivo* using STZ-induced adult diabetic mice (male C57B6, Jackson Lab, USA). Mice were treated in accordance with the Guide for Care and Use of Laboratory Animals, approved by the local committee. The blood glucose levels of mice were continuously monitored using the Clarity GL2Plus Glucose Monitor (VWR, USA) for 2 days before the experiments by collecting 3 μL of blood from the tail vein. The insulin or PBS solution was injected using a 1 cc syringe with a 19-gauge needle into the subcutaneous dorsum of mice that had been anesthetized with 1% isoflurane. The glucose levels of each mouse were monitored over time. To measure the insulin concentration *in vivo*, 25 μL of blood samples were drawn from the tail vein of mice. Five μL of serum samples were stored frozen at −20 °C until assayed. Plasma insulin concentrations were determined using the human insulin ELISA kit (Calbiotech, USA).

Statistical Analysis. All results presented were averaged and expressed as the mean $\pm$ SD. Student's *t*-test or ANOVA were utilized to determine statistical significance between different groups. A P value < 0.05 was considered to be statistically significant.

Conflict of Interest: The authors declare no competing financial interest.

Acknowledgment. This work was supported by the grants from the American Diabetes Association (ADA) (1-14-JF-29 and 1-15-ACE-21), the grant 550 KR51307 from NC TraCS, NIH's Clinical and Translational Science Awards (CTSA) at UNC−CH (1UL1TR001111) and the start-up package from the Joint BME Department of UNC−CH and NC State to Z.G., and by the National Science Foundation (NSF) through ASSIST Engineering Research Center at NC State (EEC-1160483) to Y.Z.

Supporting Information Available: The Supporting Information is available free of charge on the ACS Publications website at DOI: 10.1021/acsnano.5b03975.

Experimental details for preparation and characterization of the nanoparticles, microdepots, strain sensors, finite element analysis, *in vitro* studies and antibacterial evaluation. (PDF)

REFERENCES AND NOTES

1. Wang, Y.; Shim, M. S.; Levinson, N. S.; Sung, H. W.; Xia, Y. Stimuli-Responsive Materials for Controlled Release of Theranostic Agents. *Adv. Funct. Mater.* **2014**, *24*, 4206–4220.
2. Peer, D.; Karp, J. M.; Hong, S.; Farokhzad, O. C.; Margalit, R.; Langer, R. Nanocarriers as an Emerging Platform for Cancer Therapy. *Nat. Nanotechnol.* **2007**, *2*, 751–760.
3. Ke, C. J.; Su, T. Y.; Chen, H. L.; Liu, H. L.; Chiang, W. L.; Chu, P. C.; Xia, Y.; Sung, H. W. Smart Multifunctional Hollow Microspheres for the Quick Release of Drugs in Intracellular Lysosomal Compartments. *Angew. Chem.* **2011**, *123*, 8236–8239.
4. Ong, W.; Yang, Y.; Cruciano, A. C.; McCarley, R. L. Redox-Triggered Contents Release from Liposomes. *J. Am. Chem. Soc.* **2008**, *130*, 14739–14744.
5. Mo, R.; Jiang, T.; DiSanto, R.; Tai, W.; Gu, Z. ATP-Triggered Anticancer Drug Delivery. *Nat. Commun.* **2014**, *5*, 3364–3373.
6. Biswas, A.; Joo, K.-I.; Liu, J.; Zhao, M.; Fan, G.; Wang, P.; Gu, Z.; Tang, Y. Endoprotease-Mediated Intracellular Protein Delivery using Nanocapsules. *ACS Nano* **2011**, *5*, 1385–1394.
7. Gu, Z.; Yan, M.; Hu, B.; Joo, K.-I.; Biswas, A.; Huang, Y.; Lu, Y.; Wang, P.; Tang, Y. Protein Nanocapsule Weaved with Enzymatically Degradable Polymeric Network. *Nano Lett.* **2009**, *9*, 4533–4538.
8. Ravaine, V.; Ancla, C.; Catargi, B. Chemically Controlled Closed-Loop Insulin Delivery. *J. Controlled Release* **2008**, *132*, 2–11.
9. Gu, Z.; Aimetti, A. A.; Wang, Q.; Dang, T. T.; Zhang, Y.; Veiseh, O.; Cheng, H.; Langer, R. S.; Anderson, D. G. Injectable Nano-Network for Glucose-Mediated Insulin Delivery. *ACS Nano* **2013**, *7*, 4194–4201.
10. Zhang, Y.; Yin, Q.; Yin, L.; Ma, L.; Tang, L.; Cheng, J. Chain-Shattering Polymeric Therapeutics with On-Demand Drug-Release Capability. *Angew. Chem., Int. Ed.* **2013**, *52*, 6435–6439.
11. Choi, S. W.; Zhang, Y.; Xia, Y. A Temperature-Sensitive Drug Release System Based on Phase-Change Materials. *Angew. Chem., Int. Ed.* **2010**, *49*, 7904–7908.
12. Huebsch, N.; Kearney, C. J.; Zhao, X.; Kim, J.; Cezar, C. A.; Suo, Z.; Mooney, D. J. Ultrasound-Triggered Disruption and Self-Healing of Reversibly Cross-Linked Hydrogels for Drug Delivery and Enhanced Chemotherapy. *Proc. Natl. Acad. Sci. U. S. A.* **2014**, *111*, 9762–9767.

13. Oliveira, H.; Perez-Andres, E.; Thevenot, J.; Sandre, O.; Berra, E.; Lecommandoux, S. Magnetic Field Triggered Drug Release from Polymersomes for Cancer Therapeutics. *J. Controlled Release* **2013**, *169*, 165–170.
14. Zhao, X.; Kim, J.; Cezar, C. A.; Huebsch, N.; Lee, K.; Bouhadir, K.; Mooney, D. J. Active Scaffolds for On-Demand Drug and Cell Delivery. *Proc. Natl. Acad. Sci. U. S. A.* **2011**, *108*, 67–72.
15. Kwon, I. C.; Bae, Y. H.; Kim, S. W. Electrically Erodible Polymer Gel for Controlled Release of Drugs. *Nature* **1991**, *354*, 291–3.
16. Lu, Y.; Sun, W.; Gu, Z. Stimuli-Responsive Nanomaterials for Therapeutic Protein Delivery. *J. Controlled Release* **2014**, *194*, 1–19.
17. Lee, K. Y.; Peters, M.; Mooney, D. Controlled Drug Delivery from Polymers by Mechanical Signals. *Adv. Mater.* **2001**, *13*, 837–839.
18. Lee, K. Y.; Peters, M. C.; Anderson, K. W.; Mooney, D. J. Controlled Growth Factor Release from Synthetic Extracellular Matrices. *Nature* **2000**, *408*, 998–1000.
19. Izawa, H.; Kawakami, K.; Sumita, M.; Tateyama, Y.; Hill, J. P.; Ariga, K. β-Cyclodextrin-Crosslinked Alginate Gel for Patient-Controlled Drug Delivery Systems: Regulation of Host-Guest Interactions with Mechanical Stimuli. *J. Mater. Chem. B* **2013**, *1*, 2155–2161.
20. Hyun, D. C.; Moon, G. D.; Park, C. J.; Kim, B. S.; Xia, Y.; Jeong, U. Strain-Controlled Release of Molecules from Arrayed Microcapsules Supported on an Elastomer Substrate. *Angew. Chem., Int. Ed.* **2011**, *50*, 724–727.
21. Yao, S.; Zhu, Y. Nanomaterial-Enabled Stretchable Conductors: Strategies, Materials and Devices. *Adv. Mater.* **2015**, *27*, 1480–1511.
22. Kim, D.-H.; Lu, N.; Ma, R.; Kim, Y.-S.; Kim, R.-H.; Wang, S.; Wu, J.; Won, S. M.; Tao, H.; Islam, A. Epidermal Electronics. *Science* **2011**, *333*, 838–843.
23. Takei, K.; Takahashi, T.; Ho, J. C.; Ko, H.; Gillies, A. G.; Leu, P. W.; Fearing, R. S.; Javey, A. Nanowire Active-Matrix Circuitry for Low-Voltage Macroscale Artificial Skin. *Nat. Mater.* **2010**, *9*, 821–826.
24. Minev, I. R.; Musienko, P.; Hirsch, A.; Barraud, Q.; Wenger, N.; Moraud, E. M.; Gandar, J.; Capogrosso, M.; Milekovic, T.; Asboth, L.; *et al.* Electronic Dura Mater for Long-Term Multimodal Neural Interfaces. *Science* **2015**, *347*, 159–163.
25. Gu, Z.; Dang, T. T.; Ma, M.; Tang, B. C.; Cheng, H.; Jiang, S.; Dong, Y.; Zhang, Y.; Anderson, D. G. Glucose-Responsive Microgels Integrated with Enzyme Nanocapsules for Closed-Loop Insulin Delivery. *ACS Nano* **2013**, *7*, 6758–6766.
26. Mørch, Ý. A.; Donati, I.; Strand, B. L.; Skjåk-Bræk, G. Effect of Ca^{2+}, Ba^{2+}, and Sr^{2+} on Alginate Microbeads. *Biomacromolecules* **2006**, *7*, 1471–1480.
27. Dragon Skin Data Sheets. http://www.smooth-on.com/tb/files/DRAGON_SKIN_SERIES_TB.pdf; http://www.smooth-on.com/msds/files/BD_DS_Eco_Equ_EZB_EZS_Psy_MS_OOMOO_Reb_ST_SS_Soma_Sol_Sorta.pdf (accessed September 9, 2014).
28. Yao, S.; Zhu, Y. Wearable Multifunctional Sensors using Printed Stretchable Conductors Made of Silver Nanowires. *Nanoscale* **2014**, *6*, 2345–2352.
29. Wessendorf, A. M.; Newman, D. J. Dynamic Understanding of Human-Skin Movement and Strain-Field Analysis. *IEEE Trans. Biomed. Eng.* **2012**, *59*, 3432–3438.
30. Bird, R. B.; Stewart, W. E.; Lightfoot, E. N. *Transport Phenomena*; John Wiley & Sons: New York, 2007; pp 780−786.
31. Jaeger, R. C. *Introduction to Microelectronic Fabrication*, 2nd ed.; Prentice Hall: Upper Saddle River, NJ, 2002; pp 220−232.
32. Sparks, J. L.; Vavalle, N. A.; Kasting, K. E.; Long, B.; Tanaka, M. L.; Sanger, P. A.; Schnell, K.; Conner-Kerr, T. A. Use of Silicone Materials to Simulate Tissue Biomechanics as Related to Deep Tissue Injury. *Adv. Skin Wound Care* **2015**, *28*, 59–68.
33. Wang, C.; Cowen, C.; Zhang, Z.; Thomas, C. High-Speed Compression of Single Alginate Microspheres. *Chem. Eng. Sci.* **2005**, *60*, 6649–6657.
34. Mo, R.; Jiang, T.; Di, J.; Tai, W.; Gu, Z. Emerging Micro-and Nanotechnology based Synthetic Approaches for Insulin Delivery. *Chem. Soc. Rev.* **2014**, *43*, 3595–3629.
35. Prausnitz, M. R. Microneedles for Transdermal Drug Delivery. *Adv. Drug Delivery Rev.* **2004**, *56*, 581–587.
36. Prausnitz, M. R.; Langer, R. Transdermal Drug Delivery. *Nat. Biotechnol.* **2008**, *26*, 1261–1268.
37. Yu, J.; Zhang, Y.; Ye, Y.; DiSanto, R.; Sun, W.; Ranson, D.; Ligler, F. S.; Buse, J. B.; Gu, Z. Microneedle-Array Patches Loaded with Hypoxia-Sensitive Vesicles Provide Fast Glucose-Responsive Insulin Delivery. *Proc. Natl. Acad. Sci. U. S. A.* **2015**, *112*, 8260–8265.
38. Holst, J. J. The Physiology of Glucagon-Like Peptide 1. *Physiol. Rev.* **2007**, *87*, 1409–1439.
39. Son, D.; Lee, J.; Qiao, S.; Ghaffari, R.; Kim, J.; Lee, J. E.; Song, C.; Kim, S. J.; Lee, D. J.; Jun, S. W. Multifunctional Wearable Devices for Diagnosis and Therapy of Movement Disorders. *Nat. Nanotechnol.* **2014**, *9*, 397–404.
40. Honda, W.; Harada, S.; Arie, T.; Akita, S.; Takei, K. Wearable, Human-Interactive, Health-Monitoring, Wireless Devices Fabricated by Macroscale Printing Techniques. *Adv. Funct. Mater.* **2014**, *24*, 3299–3304.
41. Mitragotri, S.; Anderson, D.; Chen, S.; Chow, E.; Ho, D.; Kabanov, A.; Karp, J.; Kataoka, K.; Mirkin, C.; Petrosko, S.; *et al.* Accelerating the Translation of Nanomaterials in Biomedicine. *ACS Nano* **2015**, *9*, 6644–6654.
42. Jiang, T.; Mo, R.; Bellotti, A.; Zhou, J.; Gu, Z. Gel-Liposome-Mediated Co-Delivery of Anticancer Membrane-Associated Proteins and Small-Molecule Drugs for Enhanced Therapeutic Efficacy. *Adv. Funct. Mater.* **2014**, *24*, 2295–2304.